

This document was prepared in conjunction with work accomplished under Contract No. DE-AC09-76SR00001 with the U.S. Department of Energy.

DISCLAIMER

This report was prepared as an account of work sponsored by an agency of the United States Government. Neither the United States Government nor any agency thereof, nor any of their employees, makes any warranty, express or implied, or assumes any legal liability or responsibility for the accuracy, completeness, or usefulness of any information, apparatus, product or process disclosed, or represents that its use would not infringe privately owned rights. Reference herein to any specific commercial product, process or service by trade name, trademark, manufacturer, or otherwise does not necessarily constitute or imply its endorsement, recommendation, or favoring by the United States Government or any agency thereof. The views and opinions of authors expressed herein do not necessarily state or reflect those of the United States Government or any agency thereof.

This report has been reproduced directly from the best available copy.

Available for sale to the public, in paper, from: U.S. Department of Commerce, National Technical Information Service, 5285 Port Royal Road, Springfield, VA 22161, phone: (800) 553-6847, fax: (703) 605-6900, email: orders@ntis.fedworld.gov online ordering: <http://www.ntis.gov/ordering.htm>

Available electronically at <http://www.doe.gov/bridge>

Available for a processing fee to U.S. Department of Energy and its contractors, in paper, from: U.S. Department of Energy, Office of Scientific and Technical Information, P.O. Box 62, Oak Ridge, TN 37831-0062, phone: (865) 576-8401, fax: (865) 576-5728, email: reports@adonis.osti.gov

ACC. NO. 142298

CC: J. M. Boswell
W. W. F. Yau
R. L. Frontroth
D. R. Leader
E. T. Booth
TIS File Copy

M E M O R A N D U M

April 22, 1980

TO: G. F. MERZ

**TIS FILE
RECORD COPY**

FROM: R. S. STOUGHTON* - H. B. PEACOCK

AN EXPERIMENTAL ANALYSIS OF CRACKING DURING EXTRUSION

INTRODUCTION

Central bursting and/or surface tearing occur during extrusion of SRP reactor fuel tubes with high wt % U cores. Cracking takes place when the maximum effective strain in the billet exceeds a critical value which is dependent on the mechanical properties of the material. The maximum effective strain is a function of extrusion parameters, such as reduction ratio, die geometry, and temperature. A quantitative analysis of cracking will result in cost savings because high wt % tubes can be made with high fabrication yields.

SUMMARY

A technique for applying grids to billet halves to study deformation during extrusion was developed. The technique uses a rubber stamp with a twenty-line-per-inch grid and special high temperature ink. It gives a grid having ± 0.005 inch accuracy. Inserting a copper screen inside the billet was evaluated but did not give accurate data because the original grid was not sufficiently square.

A method for calculating strains from large deformations has been developed and is used to calculate the principal strains in the billet. Contour graphs of the strains are also plotted.

Conditions which cause cracking during extrusion are being determined. Several tests were done using Mg-Al alloy and DU_3O_8 -Al powder metallurgy billets. Surface tearing was observed for both Mg-Al and DU_3O_8 -Al; however, central bursting has not been observed.

* Co-op Student, University of Tennessee

An extensometer was designed for high temperature tensile tests to determine the stress-strain behavior of core materials at extrusion temperatures (200-400°C). The extensometer has two rods to transfer the elongation of the specimen gauge length from the high temperature chamber to linear variable differential transformers (LVDT) located outside the furnace.

DISCUSSION

A complete study of the phenomenon of cracking must include an analysis of the effective strain ($\bar{\epsilon}$) distribution as a function of extrusion parameters such as die angle, temperature, extrusion ratio, and lubrication. From the data, optimum extrusion conditions can be determined which will minimize the maximum effective strain at the die exit. Also, the critical effective strain that causes surface tearing and central bursting can be interpolated from the data once conditions for tearing are established.

The critical effective strain values can be determined experimentally as a function of temperature from uniaxial tensile tests. These values can be compared with critical values determined from billet extrusions. Tensile tests will also provide stress-strain data for the core materials. From the stress-strain data, the stress distribution during extrusion can be approximated.

Grid Technique

Strain data for extrusion are obtained from a grid placed inside a billet before extrusion. A stamped grid (see Figure 1) proved to be the quickest and easiest method of obtaining accurate data. Inserting a piece of copper screen was tried, but this technique did not give good data because the screen resists deformation and the grid was not square.

For the ink stamp technique, a billet 3.25 inches in diameter and four inches long was cut in half lengthwise. The inside surface was milled smooth and cleaned. A high temperature resistant ink* was used to stamp a twenty-line-per-inch grid onto the inside surface of the billet. A fifty-line-per-inch stamp was tested but the grid was too small to get a good imprint. Reduced copper powder (-325 mesh) was sprinkled onto the wet ink to improve contrast. After the ink dried, the excess powder was blown off with compressed air. The billet halves were welded together, all the way around, to prevent extrusion lubricant from disturbing the grid. The billet was extruded about halfway (enough for the flow field to be fully established) and removed from the die. After cooling, it was carefully split apart and photographs taken of the deformed grid (see Figure 2). The photographs were enlarged and the coordinates of the grid intersection recorded with the digitizer. This technique gave accurate data (± 0.005 inch).

In reviewing the literature,⁽¹⁾ other grid techniques were found but were not tested. Machining a grid onto the inside surface of the billet is time consuming and may affect the results as it would create stress concentrations. Photographically etching a grid onto the billet surface was not pursued.

* Letterpress Ink, Phillips Process Co., Inc.

Strain Calculations

Strains are calculated from the coordinates of the deformed grid. The grid deformations are quite large, so assumptions based on small-scale deformation dealt with in linear elasticity are not valid. For large deformations, strains can be found by matrix algebra⁽²⁾ (see Appendix A). The only assumption made is that the grid deformation is homogeneous, i.e., straight lines in the undeformed grid remain straight, and parallel lines remain parallel. This assumption is true provided the grid size is sufficiently small. In our case, it is found to be reasonable for all but a very few data points at the die corners.

Data are put into a computer program⁽³⁾ which plots the strain fields (see Figure 3). The maximum effective strain can be easily determined over the entire billet surface.

Types of Cracking

In general, the effective strain for an extruded rod is greatest at the surface, decreasing to a minimum along the axis.⁽⁴⁾ However, under certain conditions a local maximum appears just outside the axis giving a double maximum flow. Strains near the surface of the rod are essentially shear and shifts gradually to pure tensile near the axis. There are two basic types of cracking: 1) surface tearing, and 2) central bursting. Surface tearing begins at the surface of the extruded rod propagating inward and is caused when the shear strain exceeds a critical value. Central bursting initiates at or near the axis of extrusion and is caused by inordinately high tensile strains along or near the axis. These two very different types of cracking must be avoided for successful fuel tube extrusion.

Conditions Causing Cracking

The conditions under which both types of cracking first occurs are being sought. This will enable a study of the strain fields leading up to cracking. Extrusions have been done with a 3.25-inch-diameter 1100 aluminum billet using various dies and temperatures. The Fab Lab extrusion press does not have enough force (maximum 520 tons) to push billets at temperatures below 220°C with a 45° one-inch die exit, and 1100 aluminum is too ductile at this temperature to crack under the stated conditions. Alloying magnesium with aluminum reduces the ductility considerably. Magnesium aluminum billets with up to 4 wt % Mg were available, but were also too ductile to crack at the lowest possible temperatures. A 30 wt % Mg-Al material was available for extrusion. This material was extremely brittle and surface tearing was observed for all extrusions including minimum conditions (365°C, 30° 2.009-inch dia).^{*} Cracks propagated directly inward, perpendicular to the surface. The literature⁽⁵⁾ refers to this as radial cracking which occurs only in the most brittle material.

* 365°C is maximum safe temperature for extruding 30% Mg-Al.

2.009" diameter is largest die in the Fab Lab; extrusion ratio = $\frac{3.25}{2.009} = 2.62$.

Billets of 50, 60, and 70 wt % $\text{DU}_3\text{O}_8\text{-Al}$ were compacted and extruded. The billets were about 3.15-inch diameter and four inches high. With the 50 wt % DU_3O_8 , surface tearing occurred at 250°C with a one-inch 45° die. The cracks occurred only in the last six inches of the extruded rod. With 60 wt %, the cracks appeared in the last six inches of the extruded rod using the same die at 325°C. The cracks propagated inward at an angle inclined to the surface of the rod. The literature⁽⁵⁾ refers to this as fir tree cracking which occurs in semibrittle material.

Effect of Die Angle

One series of extrusions has been completed. In this series, 1100 aluminum was extruded at 250°C through an approximately 1-inch die exit. The die angle α was varied. The maximum effective strain (see Figure 4) increases linearly with the die angle until a critical value (in our case ~65° half angle) is reached after the strain becomes constant. Above the critical angle, the material begins to form a dead zone.

Relationship Between Solid and Tube Extrusion

Thus far, all extrusions have been done with solid billets because experimental and theoretical data are available in the literature for comparison. The literature⁽⁶⁾ shows that the flow fields are very similar to those observed in our solid billet extrusions.

Consider a cross section of an extruded tube. The maximum effective strain occurs at the outer surface and decreases to a minimum near the mandrel. The outer surface shows essentially shearing strain shifting gradually to a purely tensile strain at the minimum value just outside the mandrel and shifting to a combined shearing and tensile strain at the mandrel-billet interface. The magnitude of the shearing strain at the inner surface is largely a function of the interface friction. With perfect lubrication, the minimum effective strain value over the cross section (the point of purely tensile strain) occurs at the inner surface. The magnitude of the effective strain at the outer surface also depends on friction, though not as greatly as on the inner surface. These similarities lead us to believe that the relationship between effective strain and the various extrusion parameters determined by solid billet extrusion will be applicable to tube extrusion.

In SRP reactor fuel tube extrusion, the core material flows through a region of combined shear and tensile deformation. Metallographic examination of cracked fuel tubes indicates that cracking first occurs in the core material. Tube failure then occurs when the cladding necks and fails. However, it is not apparent whether the core cracks are caused by surface tearing, central bursting, or a combination.

Tensile Testing

Tensile tests will be made using 50, 60, and 70 wt % $\text{DU}_3\text{O}_8\text{-Al}$ powder metallurgy specimens made from compacted and extruded core material. Tests will also be made with 1100 aluminum and 2.5 wt % Mg-Al alloy specimens. These tests will be done at elevated temperatures (up to 300°C) to determine the mechanical properties of the material at the extrusion temperatures.

Elongation measurements are a problem at high temperatures and no high temperature extensometers are available at SRL. This is overcome by machining grips and rods that transfer the elongation out of the environmental chamber through a hole in the top. The movement of each rod is recorded separately with an LVDT (linear variable differential transformer). The difference between them is the elongation of the specimen. From these tests, stress-strain curves can be found for the core materials as a function of wt % uranium and temperature. Tensile tests will be carried out to fracture, thus obtaining the maximum effective strain. Correlation of tensile test data with extrusion data will give the stress distribution in the billet.

RSS/HBP:ehj

REFERENCES

1. Farmer, L. E. and Fowle, R. F. "An Experimental Procedure for Studying the Flow in Plane Strain Extrusion," Int. J. Mech. Sci., Vol 21, p 599.
2. Hsu, T. C. "A Study of Large Deformations by Matrix Algebra," J. Strain Anal, Vol 1, No. 4, 1966.
3. McClain, L. D. and Peacock, H. B. "A Computer Code for Calculating and Plotting Strains in Extruded Solid Metal Billets," DPST-80-232, February 1, 1980.
4. Hsu, T. C. "The Characteristics of Coaxial and Non-Coaxial Strain Paths," J. Strain Analysis, 1966, Vol 1, No. 3.
5. Oh, S. I., Chen, C. C., and Kobayashi, S. "Ductile Fracture in Axisymmetric Extrusion and Drawing," Trans of ASME, Vol 101, February 1979.
6. Mehta, H. S., Shabaik, A. H., and Kobayashi, S. "Analysis of Tube Extrusion," J. Engr for Ind, May 1970, p 403.
7. Pepe, J. J. "Defect Formation During Cold Hydrostatic Extrusion," Arsenal AD-778 743, April 1974.

27

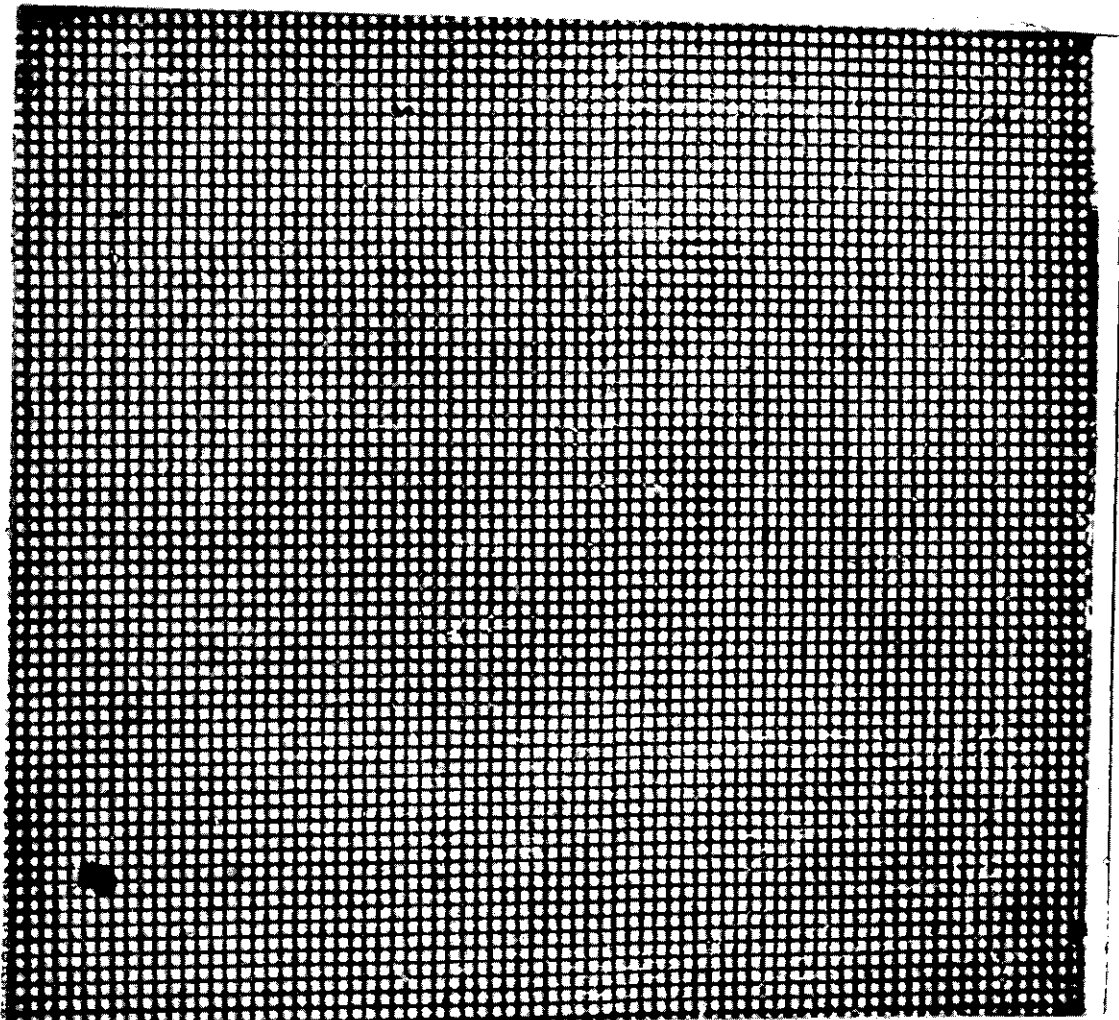


FIGURE 1. STAMPED INK GRID

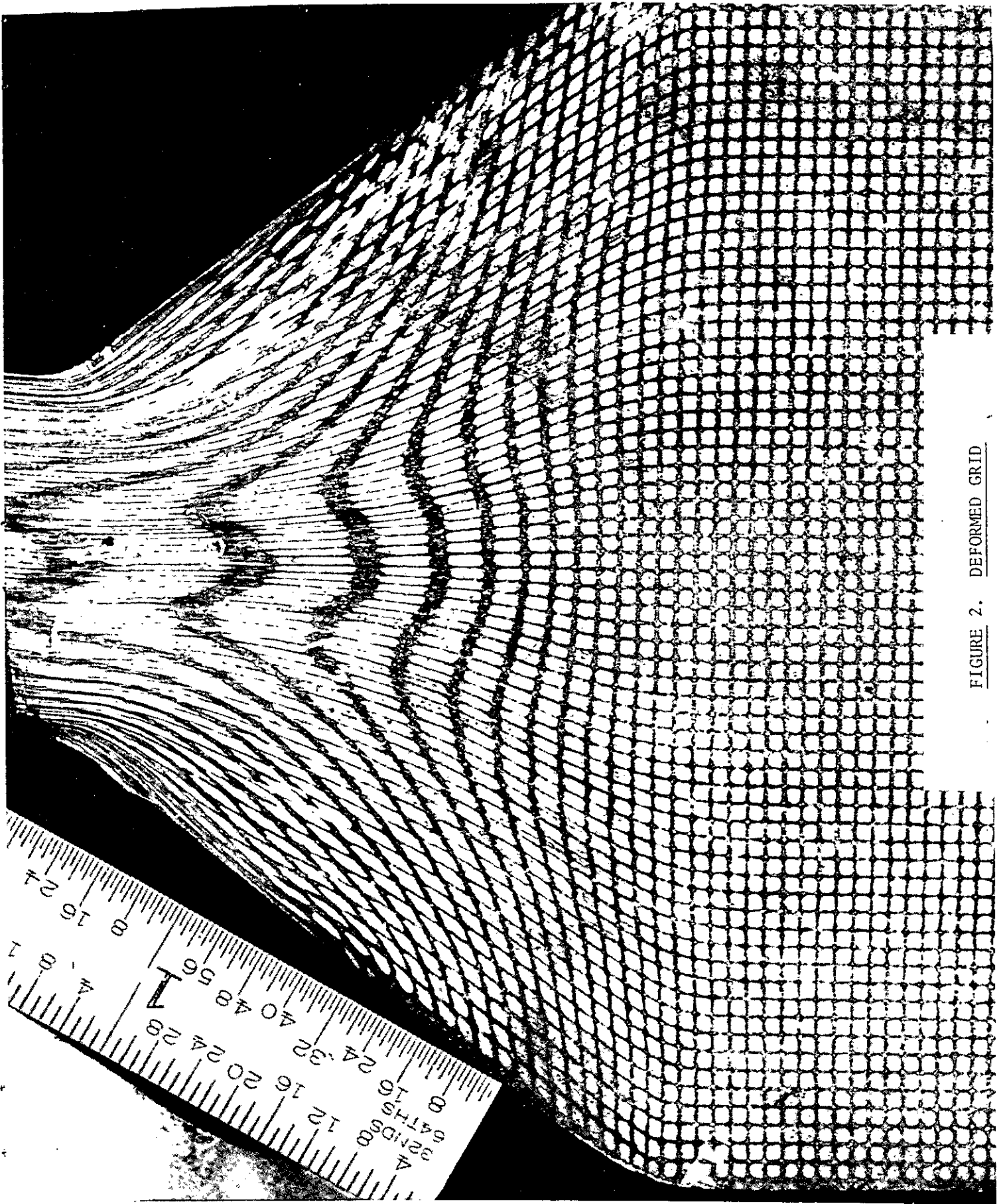


FIGURE 2. DEFORMED GRID

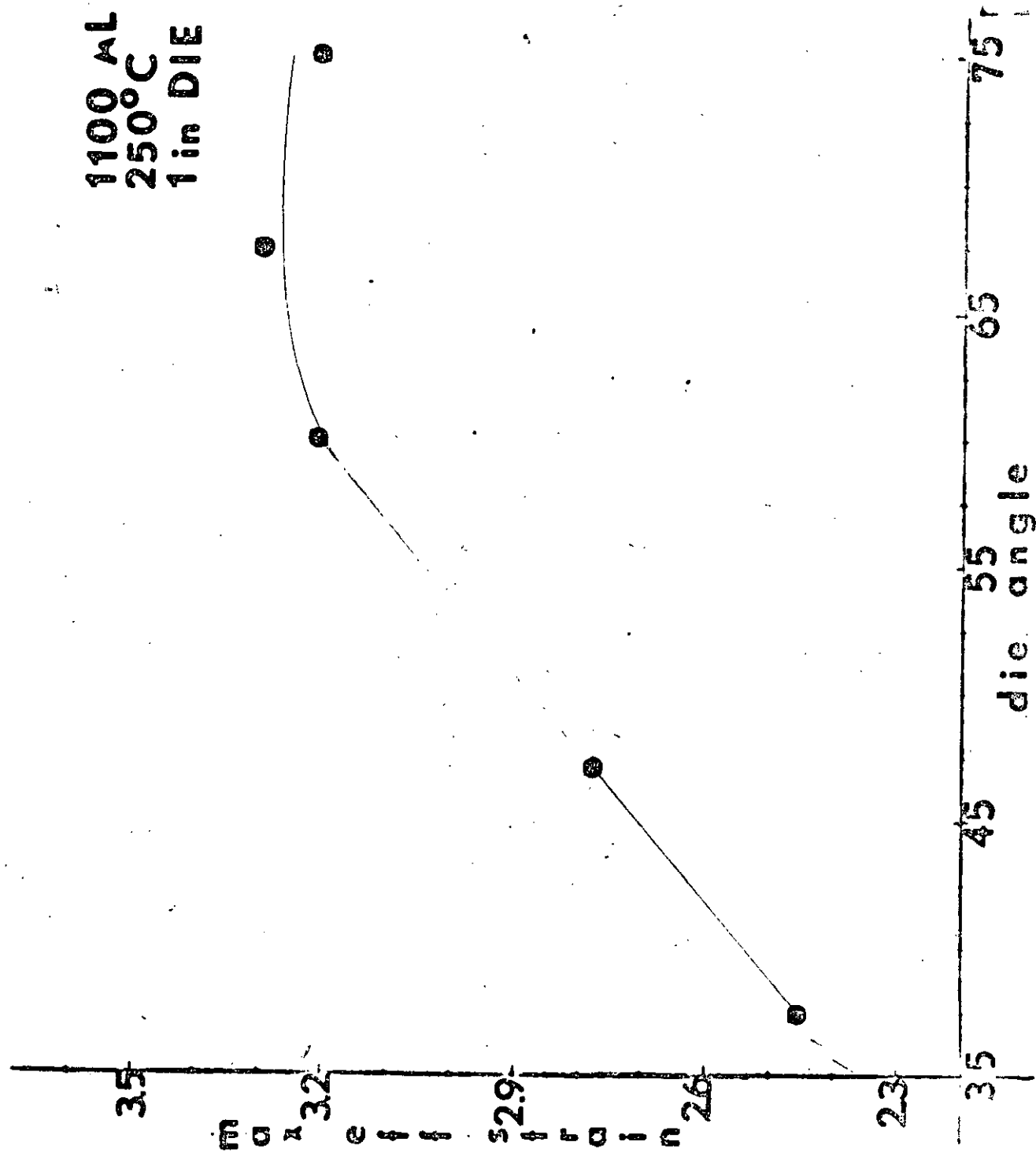


FIG. 4

APPENDIX A

ANALYSIS OF LARGE DEFORMATIONS

The mathematical techniques used to evaluate large strains are very different from those used for small strains. This is not due to any fundamental difference in the nature of small and large strains, but simply because some simplifying assumptions are valid in the analysis of small strains for engineering applications, but lead to gross errors in the analysis of large deformations. Mohr's circle relationships are not valid because they fail to take into account the strain paths and the rotation of the material particle. When two large deformations occur, the resultant deformation is dependent on the order in which they occur.

The deformation of a square grid can be represented by an affine transformation, i.e.,

$$\bar{X}'_1 = a_{11} \bar{X}_1 + a_{12} \bar{X}_2$$

$$\bar{X}'_2 = a_{21} \bar{X}_1 + a_{22} \bar{X}_2,$$

where the a's are constants and \bar{X}_1 & \bar{X}_2 are the vectors of the grid sides before deformation and \bar{X}'_1 & \bar{X}'_2 are the vectors of the grid sides after deformation. In our analysis, \bar{X}_1 is the average of the two streamline sides of a grid, and \bar{X}_2 is the average of the two transverse line sides of the grid. The only assumption made here is that the deformation of the grid is homogeneous, i.e., straight line remains straight and parallel lines remain parallel. This assumption is valid provided the grid size is sufficiently small.

Additional deformations can be represented similarly,

$$\bar{X}'_1 = b_{11} \bar{X}'_1 + b_{12} \bar{X}'_2$$

$$\bar{X}'_2 = b_{21} \bar{X}'_1 + b_{22} \bar{X}'_2$$

The deformation vectors \bar{X}'_1 & \bar{X}'_2 can be related back to the original vectors \bar{X}_1 & \bar{X}_2 by matrix multiplication,

$$\bar{X}'_1 = c_{11} \bar{X}_1 + c_{12} \bar{X}_2$$

$$\bar{X}'_2 = c_{21} \bar{X}_1 + c_{22} \bar{X}_2$$

$$\text{where } \begin{vmatrix} c_{11} & c_{12} \\ c_{21} & c_{22} \end{vmatrix} = \begin{vmatrix} b_{11} & b_{12} \\ b_{21} & b_{22} \end{vmatrix} \cdot \begin{vmatrix} a_{11} & a_{11} \\ a_{21} & a_{22} \end{vmatrix}$$

A matrix of a general two-dimensional deformation may be factored into a pure shear and a rotation, or a simple shear and a rotation, or any other way - all are equally valid. It is desirable to have a basis of comparison to refer all deformations. This choice is necessarily arbitrary. Pure shear as represented by matrix (2) is the only type of two-dimensional deformation that occurs along a coaxial strain path; that is, one in which all the incremental strains have the same principle axes with respect to the material.⁽⁴⁾ Pure shear is, therefore, a convenient standard with which to refer all deformations.

The three variables of simple shear, γ , α , and ℓ_1 , can be easily calculated from the coordinates of the grid intersections. This is expressed in matrix notation, and referred to a state of pure shear as follows (see Figure A1).

Pure shear along the reference axes is represented by the following matrix,

$$\begin{vmatrix} e^{\epsilon} & 0 \\ 0 & e^{-\epsilon} \end{vmatrix} \quad (1)$$

To describe pure shear anywhere in the plane, we may consider the deformation to be a three-step process. A rotation through an angle ϕ to the principle strain direction, the straining along the principle axes, and finally, reverse rotation through ϕ to the original reference axes. Mathematically,

$$\begin{vmatrix} \cos \phi & -\sin \phi \\ \sin \phi & \cos \phi \end{vmatrix} \cdot \begin{vmatrix} e^{\epsilon} & 0 \\ 0 & e^{-\epsilon} \end{vmatrix} \cdot \begin{vmatrix} \cos \phi & \sin \phi \\ -\sin \phi & \cos \phi \end{vmatrix}$$

The product of these matrices is,

$$\begin{vmatrix} \cosh \epsilon + \sinh \epsilon \cdot \cos 2\phi & \sinh \epsilon \cdot \sin 2\phi \\ \sinh \epsilon \cdot \sin 2\phi & \cosh \epsilon - \sinh \epsilon \cos 2\phi \end{vmatrix} \quad (2)$$

To obtain the most general matrix for pure shear strain, we must also consider the rotation of the grid during deformation. Multiplying matrix (2) by a rotation matrix,

$$\begin{vmatrix} \cos \omega & -\sin \omega \\ \sin \omega & \cos \omega \end{vmatrix} \quad (3)$$

Thus, the most general matrix for deformation of incompressible media in terms of pure shear is:

$$\begin{vmatrix} \cos \omega & -\sin \omega \\ \sin \omega & \cos \omega \end{vmatrix} \cdot \begin{vmatrix} \cosh \epsilon + \sinh \epsilon \cdot \cos 2\phi & \sinh \epsilon \cdot \sin 2\phi \\ \sinh \epsilon \cdot \sin 2\phi & \cosh \epsilon - \sinh \epsilon \cdot \sin 2\phi \end{vmatrix} \quad (4)$$

Consider a typical deformed grid as in Figure A2. The most meaningful variables we can solve for are θ , the angle to the principle strains, ϵ , the natural strain, and ω , the rotation of the grid. Consider first the deformation in Figure A3. This deformation can be considered compression along X_2 and stretching along X_1 , followed by simple shear. In matrix notation,

$$\begin{vmatrix} 1 & \gamma \\ 0 & 1 \end{vmatrix} \cdot \begin{vmatrix} \lambda_1/\lambda_0 & 0 \\ 0 & \lambda_0/\lambda_1 \end{vmatrix} \quad (5)$$

Equating this to the most general expression for pure shear,

$$\begin{vmatrix} \cos \delta & -\sin \delta \\ \sin \delta & \cos \delta \end{vmatrix} \cdot \begin{vmatrix} \cosh \epsilon + \sinh \epsilon \cos 2\theta & \sinh \epsilon \sin 2\theta \\ \sinh \epsilon \sin 2\theta & \cosh \epsilon - \sinh \epsilon \cos 2\theta \end{vmatrix} =$$

$$\begin{vmatrix} 1 & \gamma \\ 0 & 1 \end{vmatrix} \cdot \begin{vmatrix} \lambda_1/\lambda_0 & 0 \\ 0 & \lambda_0/\lambda_1 \end{vmatrix}$$

solving this we obtain the equations,

$$\cos \delta \cosh \epsilon + \cos \delta \sinh \epsilon \cos 2\theta - \sin \delta \sinh \epsilon \sin 2\theta = \lambda_1/\lambda_0 \quad (6a)$$

$$\cos \delta \sinh \epsilon \sin 2\theta - \sin \delta \cosh \epsilon + \sin \delta \sinh \epsilon \cos 2\theta = \gamma \lambda_0/\lambda_1 \quad (6b)$$

$$\cos \delta \sinh \epsilon \sin 2\theta + \sin \delta \cosh \epsilon + \sin \delta \sinh \epsilon \cos 2\theta = 0 \quad (6c)$$

$$\cos \delta \cosh \epsilon - \cos \delta \sinh \epsilon \cos 2\theta + \sin \delta \sinh \epsilon \sin 2\theta = \lambda_0/\lambda_1 \quad (6d)$$

$$(6a) + (6d) + 2 \cos \delta \cosh \varepsilon = \frac{\ell_0}{\ell_1} + \frac{\ell_1}{\ell_0} \quad (7)$$

$$(6b) - (6c) = -2 \sin \delta \cosh \varepsilon = \gamma \frac{\ell_0}{\ell_1} \quad (8)$$

$$\text{so, } \frac{-2 \sin \delta \cosh \varepsilon}{2 \cos \delta \cosh \varepsilon} = \frac{\gamma \frac{\ell_0}{\ell_1}}{\frac{\ell_0}{\ell_1} + \frac{\ell_1}{\ell_0}}$$

$$\tan \delta = \frac{-\gamma \frac{\ell_0^2}{\ell_0^2 + \ell_1^2}}{\ell_0^2 + \ell_1^2} \quad (9)$$

$$\text{from (8), } \cosh \varepsilon = \frac{\gamma \frac{\ell_0}{\ell_1}}{-2 \ell_1 \sin \delta} \quad (10)$$

(6c) $\cot \delta$ -(6a) becomes

$$\sin 2\theta \sinh \varepsilon \left(\sin \delta + \frac{\cos^2 \delta}{\sin \delta} \right) = - \frac{\ell_1}{\ell_0}$$

$$\text{so, } \sin 2\theta = \frac{- \frac{\ell_1}{\ell_0} \sin \delta}{\sinh \varepsilon} \quad (11)$$

The above equations have all assumed incompressibility of the material, i.e., the area of the deformed grid does not change. In our case, the area does change, due to hoop strain. The equations can be easily modified if we consider the grid squares to be first increased in size due to hoop strain, and then deformed according to the equations previously described.

The hoop strain, ε_c , is given by

$$\varepsilon_c = \ln \left(\frac{R_1}{R_0} \right) \quad \text{see Figure A4}$$

$$\frac{\ell_0}{\ell'_0} = \sqrt{\frac{R_1}{R_0}} \Rightarrow \ell'_0 = \ell_0 \sqrt{\frac{R_0}{R_1}}$$

Equations (9), (10), and (11) are valid if the original grid length ℓ_0 is considered to be ℓ'_0 . To relate this back to the true original length ℓ_0 , simply multiply ℓ_0 by $\sqrt{R_0/R_1}$ wherever it appears. i.e.

$$\text{eq. (9) becomes} \quad \tan \delta = - \frac{\gamma R_0 \ell_0^2}{R_1 \ell_1^2 + R_0 \ell_0^2}$$

$$\text{eq. (10) becomes} \quad \cosh \epsilon = - \frac{\gamma \ell_0}{2 \ell_1 \sin \delta} \sqrt{R_0/R_1}$$

$$\text{and eq. (11) becomes} \quad \sin 2\theta = - \frac{\ell_1}{\ell_0} \sqrt{R_1/R_0} \frac{\sin \delta}{\sinh \epsilon}$$

ω , the total rotation, can be seen to be

$$\omega = \delta + \alpha$$

The principle strains are

$$\epsilon_{\rho_1} = \epsilon - \frac{\epsilon_c}{2}$$

$$\epsilon_{\rho_2} = -\epsilon - \frac{\epsilon_c}{2}$$

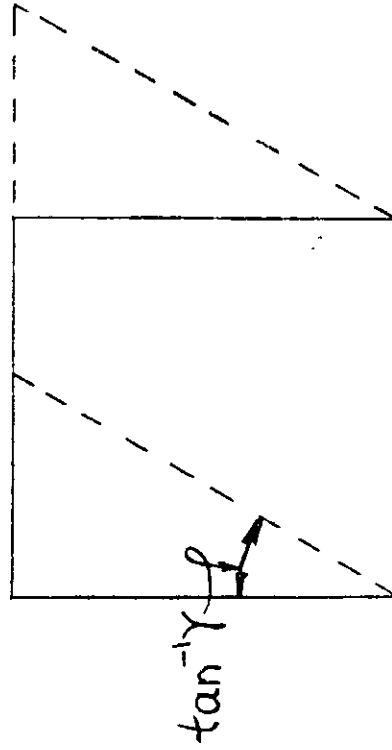
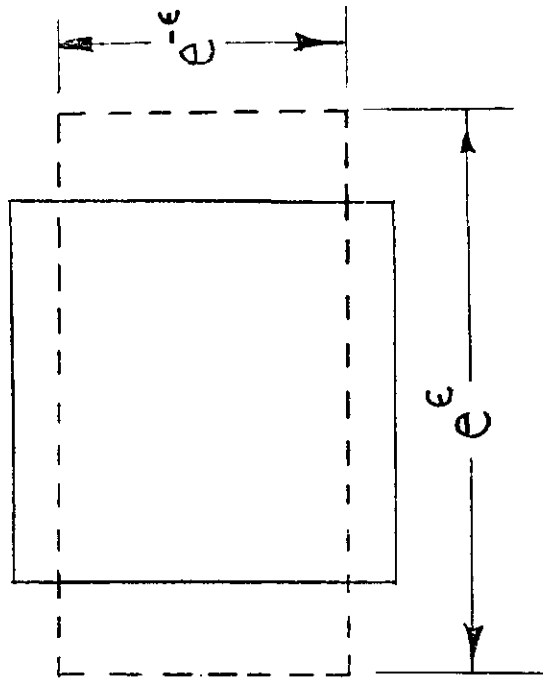
$$\epsilon_{\rho_3} = \epsilon_c$$

The effective strain is then

$$\epsilon_{\text{eff}} = \frac{1}{\sqrt{3}} \left((\epsilon_{\rho_1} - \epsilon_{\rho_2})^2 + (\epsilon_{\rho_2} - \epsilon_{\rho_3})^2 + (\epsilon_{\rho_3} - \epsilon_{\rho_1})^2 \right)^{1/2}$$

PURE SHEAR

SIMPLE SHEAR



NOTE: AXES ARE PRINCIPLE AXES

FIG. A1

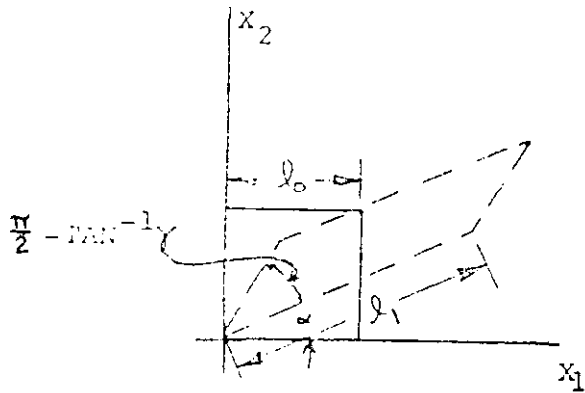


FIG. A2

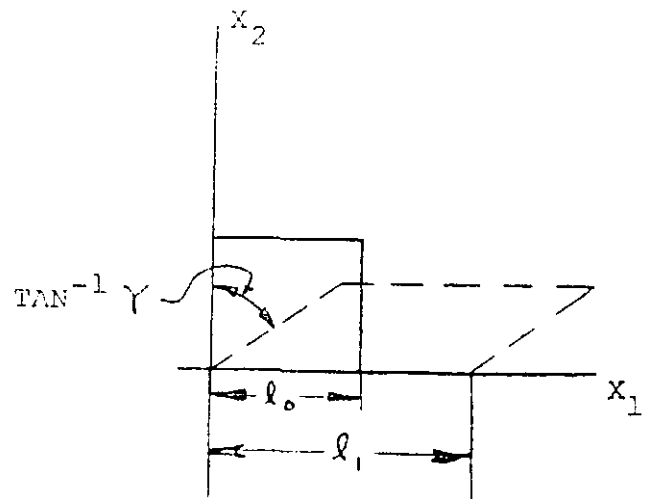


FIG. A3

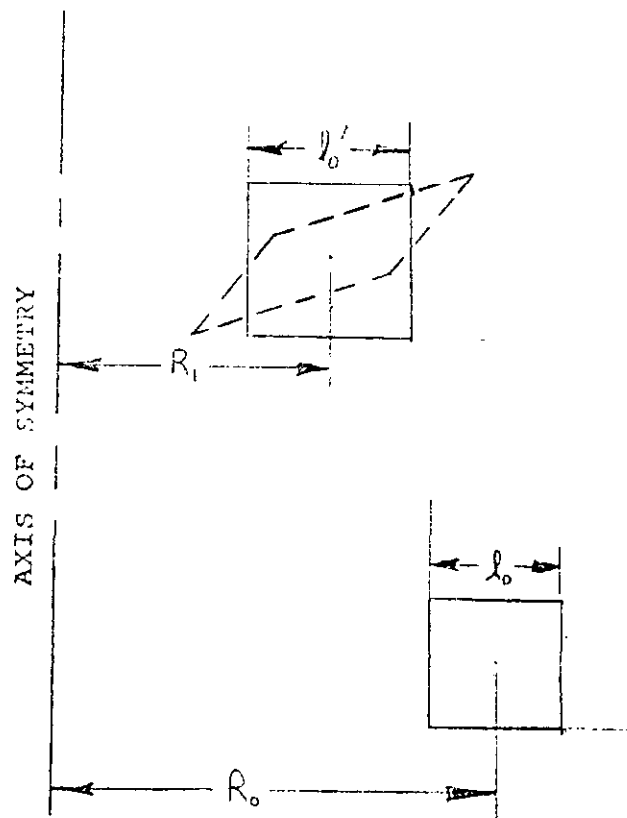


FIG. A4